ANTICANCER RESEARCH *31*: 113-122 (2011)

Constitutively Active *FGFR3* with Lys650Glu Mutation Enhances Bortezomib Sensitivity in Plasma Cell Malignancy

MASAYASU OTSUKA[1], MASAO MIZUKI[1], JIRO FUJITA[1], SUMIN KANG[2] and YUZURU KANAKURA[1]

[1]*Department of Hematology and Oncology, Osaka University Graduate School of Medicine, 2-2 Yamada-oka, Suita, Osaka 565-0871, Japan;*
[2]*Hematology/Medical Oncology, Emory University School of Medicine, Winship Cancer Institute of Emory, Atlanta, GA 30322, U.S.A.*

Abstract. *The ectopically expressed fibroblast growth factor receptor 3 (FGFR3) and its constitutively active mutations have been detected in patients with multiple myeloma (MM). This study investigated whether the cytotoxic effects of bortezomib on malignant plasma cells are associated with FGFR3 expression and the existence of mutations of FGFR3. Materials and Methods: Cell apoptosis assays were performed in a plasmacytoma cell line, FR4 cells and a myeloma cell line, RPMI8226 cells overexpressing wild-type FGFR3 ($FGFR3^{WT}$) or two different mutants, $FGFR3^{K650E}$ or $FGFR3^{Y373C}$, and the induction of endoplasmic reticulum (ER) stress protein was compared between each type of cell. Results: FR4 cells with $FGFR3^{K650E}$ showed enhanced sensitivity to bortezomib together with increased induction of ER stress proteins, compared to FR4 cells with mock, $FGFR3^{WT}$ or $FGFR3^{Y373C}$. RPMI8226 cells with $FGFR3^{K650E}$ also showed enhanced bortezomib sensitivity. Conclusion: This study indicated that FGFR3K650E is associated with bortezomib sensitivity in malignant plasma cells via ER stress pathways.*

The t(4;14)(p16.3;q32.3) translocation occurs in 15-25% of multiple myeloma (MM) patients and leads to the deregulation of *FGFR3* gene (1). This results in ectopic expression of FGFR3, which promotes the proliferation and survival in myeloma cells (2, 3). Clinical data indicate that patients with this translocation demonstrate resistance to conventional chemotherapy and early progression after a response occurs, leading to poor prognosis. It has been reported that activating mutations of *FGFR3* are found in bladder and cervical cancer (4, 5) and overexpression of FGFR3 has been observed in Hodgkin's and T-cell lymphomas (6-8), suggesting that FGFR3 is associated with the oncogenic transformation. FGFR3 is a receptor tyrosine kinase which is composed of extracellular three immunoglobulin-like domains, a single transmembrane helix and a cytoplasmic tyrosine kinase domain (9). FGFR3 has a heparin-binding site in the extracellular domain, underlying the mechanism of dimerization induced by a ligand, FGF, together with heparin (9). Activating mutations of *FGFR3*, such as Lys650Glu (K650E) and Tyr373Cys (Y373C) have been identified in MM patients with t(4;14) (10). The former exists in the activation loop of the tyrosine kinase domain and the latter in the transmembrane domain. These mutations have been reported in tumor cells from patients in the terminal therapy-refractory phase of the disease or in cell lines established from advanced diseases, suggesting that the presence of these mutations are associated with the worst prognosis (10).

Bortezomib, which was the first proteasome inhibitor to be used clinically (11, 12), was initially reported to induce apoptosis by inhibiting the activation of NF-kappaB. However, the mechanism is now revealed to be more complicated. Recently, it has been reported that the balance between proteasome workload and degradative capacity is a critical determinant of sensitivity of MM cells to proteasome inhibitors (13). In order to examine whether *FGFR3* and its mutations are associated with the cytotoxic effect of bortezomib, this study established MM cells which overexpressed wild-type FGFR3, K650E or Y373C-mutated FGFR3 and analysed their bortezomib sensitivity in relation to the ER stress.

Correspondence to: Masao Mizuki, Department of Hematology and Oncology, Osaka University Graduate School of Medicine, 2-2 Yamada-oka, Suita, Osaka 565-0871, Japan. Tel: +81 668793871, Fax: +81 668793879, e-mail: mizuki@bldon.med.osaka-u.ac.jp

Key Words: Proteasome inhibitor, receptor tyrosine kinase, activation loop, multiple myeloma, ER stress, FGFR3, Lys650Glu mutation, K650E, bortezomide, plasma cell malignancy.

Materials and Methods

DNA constructs. pMSCV-neo plasmid and two pMSCV-neo plasmids containing the full-length human complememtary DNA (cDNA) of wild-type or K650E mutant form of *FGFR3* were constructed, as previously described (14). The Y373C mutant form was created from wild-type *FGFR3* with QuikChange-XL Site-

Directed Mutagenesis Kit (Stratagene, La Jolla, CA, USA). Primer sequences for Y373C were: 5'primer GAGGCGGGCAGTGTG TGTGCAGGCATCCTCAGC and 3'primer GCTGAGGATGCCTG CACACACACTGCCCGCCTC. Mutations were confirmed by sequencing.

Cell culture and transfections. The human plasmacytoma cell line FR4 (15) and the MM cell line RPMI8226 were used in this study. These cell lines are negative for either t(4;14) or expression of endogenous FGFR3 (2). FR4 and RPMI8226 cells were cultured in RPMI-1640 medium (Nacalai Tesque, Kyoto, Japan) plus fetal calf serum (FCS) (ICN Biomedicals Inc., Aurora, Ohio, USA) and penicillin-streptomycin (100 μg/ml), and cultured at 37°C in a humidified atmosphere containing 5% CO_2. FR4 cells and RPMI8226 cells were transfected with the plasmid encoding a full length *FGFR3* cDNA of wild-type, K650E or Y373C mutations, or vector alone (mock). FR4 cells were transfected using FuGENE6 Transfection Reagent (Roche, Basel, Switzerland) according to the manufacturer's procedure. One day before the transfection, 2×10^5 cells in 2 ml of medium were plated to each well of a six-well plate. The mixture of 97 μl of serum-free medium, 3 μl of FuGENE6 Reagent and 2 μg of plasmid DNA was added to each well. RPMI8226 cells were transfected by electroporation. Briefly, 10 μg plasmid DNA was added to 6×10^6 cells, and then electroporation was performed at 300 V, 975 μF. Two days after the transfection with FuGENE or electroporation, the cells were placed in RPMI medium containing 0.8 mg/ml neomycin for selection. The cells stably expressing FGFR3 were then collected after the culture in selection medium by using BD FACSAria cell sorter with BD FACS Diva software (Becton Dickinson, Franklin Lakes, NJ, USA).

Western blots. Human anti-phosphoFGFR3 (Tyr-724) polyclonal antibody and anti-FGFR3 polyclonal antibody which recognizes the *C*-terminal FGFR3 were obtained from Santa Cruz Biotechnology (Santa Cruz, CA, USA). Cells were rinsed with cold phosphate-buffered saline (PBS), and lysed on ice in a lysis buffer (0.5 mM HEPES pH7.5, 1% (v/v) Triton X, 10% (v/v) glycerol, 150 mM NaCl, 1.5 mM $MgCl_2$, 5 mM EGTA, 100 mM NaF, 10 μg/ml pepstatin, 10 μg/ml leupeptin, 1 mM Na-orthovanadate). The samples were electrophoresed through a sodium dodecyl sulfate-polyacrylamide gel by loading equivalent amounts of protein and transferred to a nitrocellulose membrane (Immobilion-FL Transfer Membrane; Millipore, Billerica, MA, USA). The membrane was incubated with antibodies according to the manufacturer's protocol. Immunoblots were detected by Western Lightning (Becton Dickinson). The relative amounts of protein were evaluated by the densities of the bands using image Quant version 5.2 (Molecular Dynamics, Sunnyvale, CA, USA).

Immunocytochemistry. FR4 cells were rinsed once with PBS and incubated for 15 min in 4% paraformaldehide. Then the cells were permeabilized by 0.1% Triton X in PBS. After the procedure of blocking by 1% bovine serum albumin, the first antibody, which was either anti-FGFR3 antibody (Santa Cruz), anti-phosphoFGFR3 antibody (Santa Cruz) or anti-KDEL antibody (Stressgen, Brussels, Belgium), was added and incubated overnight. Then, the cells were washed with PBS and reacted with the second antibody which was either Alexa Fluor 488 goat anti-rabbit IgG (Invitrogen, Carlsbad, CA, USA) or Alexa Fluor 568 goat anti-mouse IgG (Invitrogen) and together with Hoechst (1 ng/ml). After washing, analyses were performed using confocal microscopy, Zeiss LSM 5 PASCAL Laser Module 405 (Carl Zeiss, Oberkochen, Germany). Two treatments were considered before analysis: (i) Brefeldin A (Sigma, St. Louis, MO, USA) treatment with a dose of 5 μg/ml for 2 hours at 37°C and (ii) FGF ligand treatment with FGF9 (100 ng/ml) and heparin (100 μg/ml) for 10 minutes at 37°C before analysed.

Apoptosis analysis. Annexin V assay was performed to evaluate the cytotoxicity of several compounds, including melphalan (Sigma), dexamethasone (Sigma) or bortezomib (Millenium Pharmaceuticals, Cambridge, MA, USA). The cells were seeded into 12-well microculture plates at 1×10^5 cells/well and incubated with each compound. After 48 hours, the cells were washed and resuspended in the binding buffer. Then 5 μl mixture of annexin V and propidium iodide was added to the cell suspension and incubated at room temperature for 5 min in the dark (Annexin V-FITC Apoptosis Detection Kit; BioVision, Mountain View, CA, USA). The cells were analyzed using BD FACSCanto II Flow Cytometer with BD FACS Diva software (Becton Dickinson).

Real-time polymerase chain reaction (PCR). Total RNA was extracted using RNeasy Mini kits (Qiagen, Germany) according to the manufacturer's instructions. cDNA was synthesized using Transcriptor First Strand cDNA Synthesis Kit (Roche). SYBR Green real-time PCR (Applied Biosystems, Carlsbad, CA, USA) was performed on cDNA extracted from cells after bortezomib treatment. The housekeeping gene *GAPDH* served as a control for the cDNA quality. The expression levels of *BIP, CHOP* and *EDEM1* were divided by the *GAPDH* expression levels, which were then used as the relative mRNA expression. Primer sequences were as follows: *BIP*, forward primer 5'-CAATCAAGGTCTATGAAGGTGAAAGA-3', reverse primer 5'-CACATCTATCTCAAAGGTGACTTCAATC-3'; *CHOP*, forward primer 5'-TGGAAATGAAGAGGAAGAATCAAAA-3', reverse primer 5'-CAGCCAAGCCAGAGAAGCA-3'; *EDEM1*, forward primer 5'-ACTCCAGCTCCAACTGCAATC-3', reverse primer 5'-GGTCAATCTGTCGCATGTAGATG-3'; and *GAPDH*, forward primer 5'-GCACCGTCAAGGCTGAGAAC-3', reverse primer 5'-TGGTGAAGACGCCAGTGGA-3'. Thermal cycling conditions were one cycle of 95°C for 10 minutes, 40 cycles of 95°C for 15 seconds and 60°C for 1 minute. Data analysis was completed using the 7500 Sequence Detection software (Applied Biosystems).

Statistical analysis. All experiments were repeated at least three times. The values reported here is the mean±standard deviation of triplicate experiments. Student's *t*-test was used to examine the statistical significance in cell apoptosis assay and real-time PCR assay. Microsoft Excel software (Microsoft, Redmond, WA, USA) was used for statistical analyses.

Results

Overexpression of wild-type, K650E and Y373C FGFR3 in FR4 and RPMI8226 cells. FR4 and RPMI8226 cells were transfected with the vector alone, or the plasmid encoding the human wild-type *FGFR3*, or *FGFR3* with K650E or Y373C mutation. These cells were named as mock-FR4, wt-FR4, KE-FR4, YC-FR4, mock-RPMI, wt-RPMI, KE-RPMI and YC-RPMI, respectively. The expression of FGFR3 was confirmed by both Western blots (Figure 1A, B) and flow

cytometry (data not shown). Cells were starved overnight and treated with or without FGF9 (100 ng/ml) and heparin (10 μg/ml) for 10 minutes before being lysed, and protein extracts were immunoprecipitated with anti-FGFR3 antibody and analyzed. As shown in Figure 1A and B, FGFR3 was not detected by Western blot in mock cells, whereas it was highly expressed in wild-type, and K650E and Y373C transfectants. This result indicated that overexpression of FGFR3 may be achieved in FGFR3-deficient cells through plasmid transfection. Western blots stained with anti-phospho-FGFR3 antibody demonstrated that K650E FGFR3 ($FGFR3^{K650E}$) and Y373C FGFR3 ($FGFR3^{Y373C}$) were autophosphorylated constitutively, while wild-type FGFR3 ($FGFR3^{WT}$) was phosphorylated only in the presence of ligand.

Localization of the FGFR3 within the cells. Immunocytochemical analysis was performed in order to visualize the localization of the FGFR3 receptors in the cells. The ER was visualized with anti-KDEL antibody which detected ER-resident proteins specifically. The images of Figure 2A show that receptors of the $FGFR3^{K650E}$ mutant were preferentially located in the ER, whereas $FGFR3^{WT}$ and $FGFR3^{Y373C}$ receptors existed on the cell surface. When the cells were treated with brefeldin A, an inhibitor of trafficking of proteins from ER-Golgi to cell surface, all FGFR3 receptors remained at the ER (Figure 2B). Since the receptor tyrosine kinase is glycosylated in the ER and the Golgi for maturation after the synthesis in the ER, the FGFR3 receptors localized in the ER are supposed to be immature forms. Positive staining with phospho-FGFR3 antibody was detected in KE- and YC-FR4 cells in the absence of the ligand, which is consistent with their constitutive activation, while it was observed in wild-type FR4 cells only after the stimulation by FGF ligand (Figure 2C, D). In addition, phospho-FGFR3 was mostly localized at the ER in KE-FR4 cells, while it was predominantly detected at the cell membrane in YC-FR4 cells and ligand-stimulated wild-type FR4 cells. These results indicated that the trafficking of $FGFR3^{K650E}$ receptor is specifically impaired and the receptor is aberrantly activated in the ER.

Bortezomib sensitivity in mock cells and FGFR3 transfectants. To evaluate the sensitivity against melphalan, dexamethasone, bortezomib and irradiation, each transfectant, as well as the mock cells, were treated with the respective agent or irradiation, and then the annexin V assay was performed. As shown in Figure 3, the cell survival decreased in a dose-dependent manner after treatment with each agent or irradiation in *FGFR3*-transfected and mock cells. There was no significant difference in the ratio of apoptosis between each cell type after the treatment with melphalan or dexamethasone (Figure 3A, B). In addition, there was no significant difference after irradiation (Figure 3C). On the contrary, the survival of

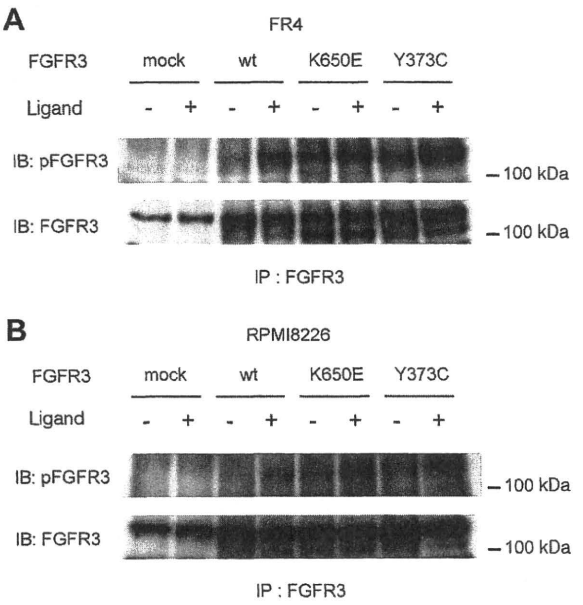

Figure 1. *FR4 (A) and RPMI8226 (B) cells transfected with mock (vector alone), wild-type (wt), K650E or Y373C FGFR3 mutants. Cell lysates were immunoprecipitated (IP) with anti-FGFR3 antibodies. Cells were treated (+) or not (–) with ligand before being lysed in buffer. The mature 130-kDa and immature 120-kDa forms are indicated.*

KE-FR4 cells declined more rapidly after exposure to bortezomib as compared to the wt- and YC-FR4 cells. As shown in Figure 3D, 52% of wt-FR4 cells and 59% of YC-FR4 cells survived 48 hours after exposure to 15 nM bortezomib, whereas only 35% of mock-FR4 cells and 19% of KE-FR4 cells survived under the same conditions. Similar results were obtained when RPMI8226 cells were used in place of FR4 cells (Figure 3E, F). These data suggest that the $FGFR3^{K650E}$ expressing cells are notably sensitive to bortezomib as compared to the cells with $FGFR3^{WT}$ and $FGFR3^{Y373}$, indicating that the effect of bortezomib is associated with the expression of *FGFR3* mutation.

Induction of ER stress associated protein by bortezomib treatment. In order to clarify the mechanism of the increased sensitivity of KE-FR4 and KE-RPMI to bortezomib, the ER stress pathway induced by bortezomib was investigated. To confirm the induction of ER stress and activation of unfolded protein response (UPR) by bortezomib treatment, the transcript levels of stress proteins, such as BIP, EDEM1 and CHOP were determined 24 hours after treatment with bortezomib. ER chaperone protein, BIP, was induced in all FR4 cell lines, the induction level of which was most pronounced in KE-FR4 cells. EDEM1, which promotes the ER-associated degradation pathway response, was marginally induced in all cells, while the level of its induction was

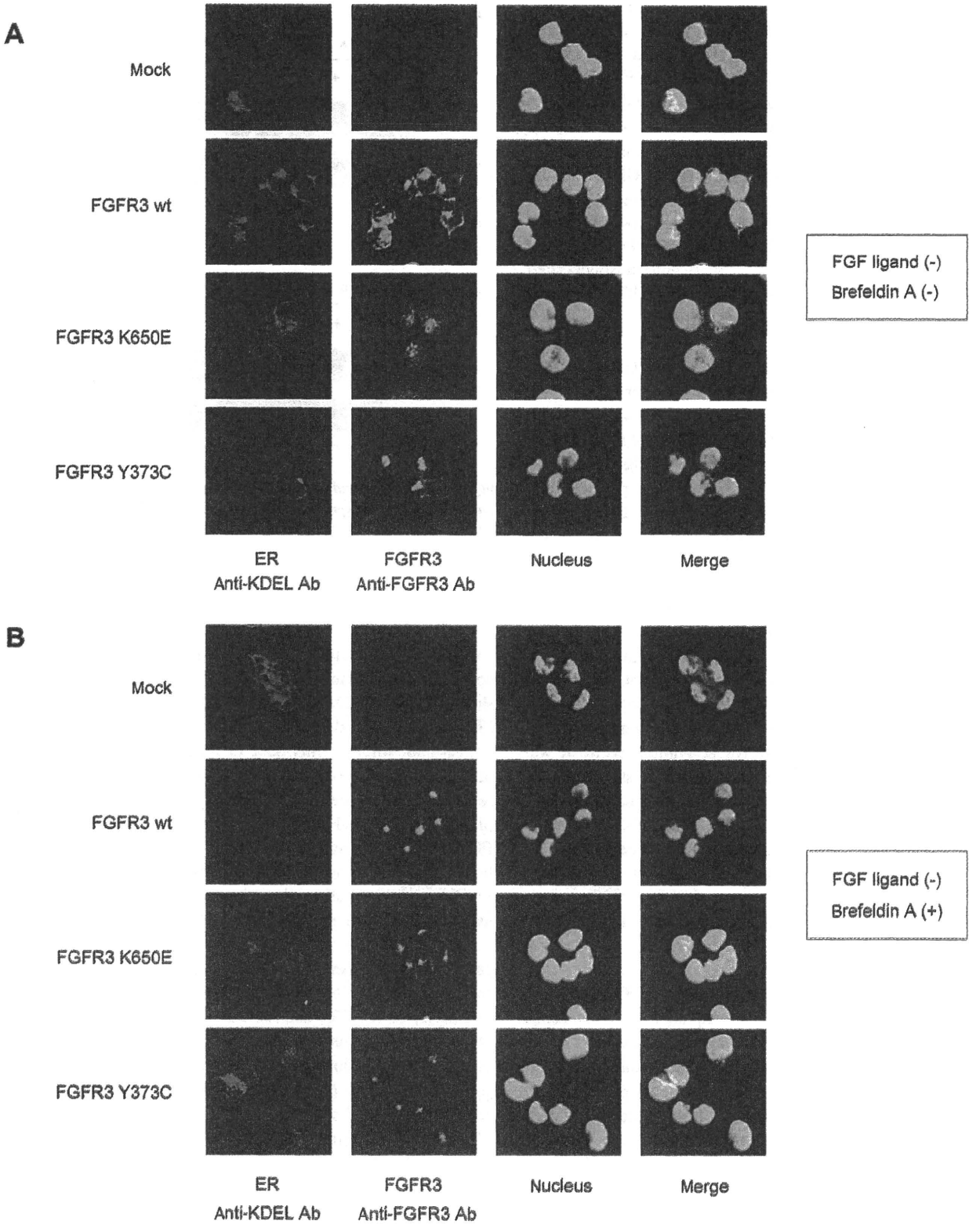

Figure 2. *continued*

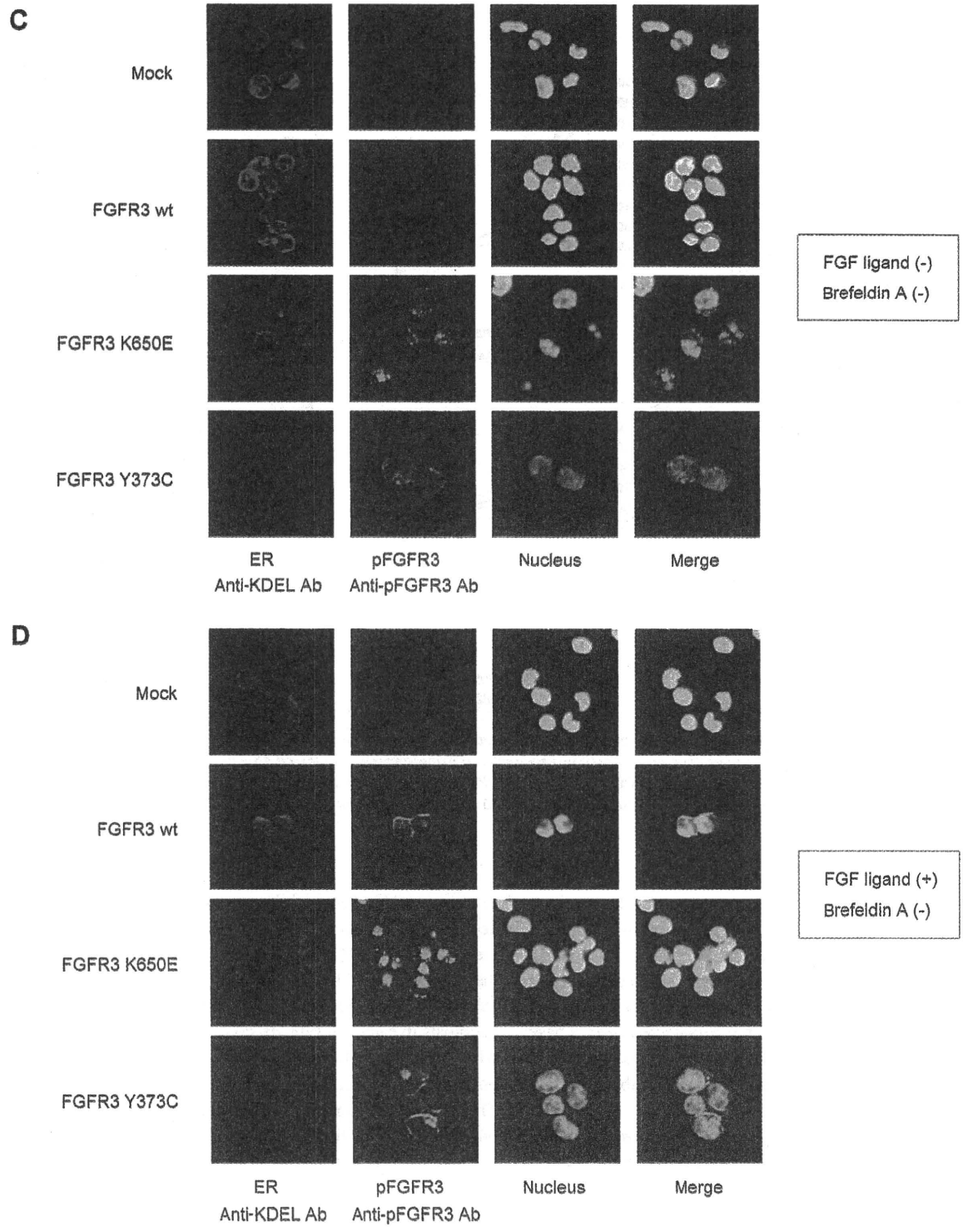

Figure 2. *Intracellular localization of wild-type (wt) and FGFR3 mutants. Cells were fixed and incubated with fluorescence-conjugated antibody. A: Merge analysis showed the presence of the wild-type and Y373C FGFR3 receptors on the cell surface. On the contrary, FGFR3 of K650E mutant were mostly located in the ER. B: FGFR3 receptors were observed within the cells when treated with brefeldin A. C: Phospho-FGFR3 receptors were detected only in the KE- and YC-FR4 cells without ligand. D: Cells after stimulation of the ligand phospho-FGFR3 receptors were detected also in wt-FR4 cells after FGF stimulation.*

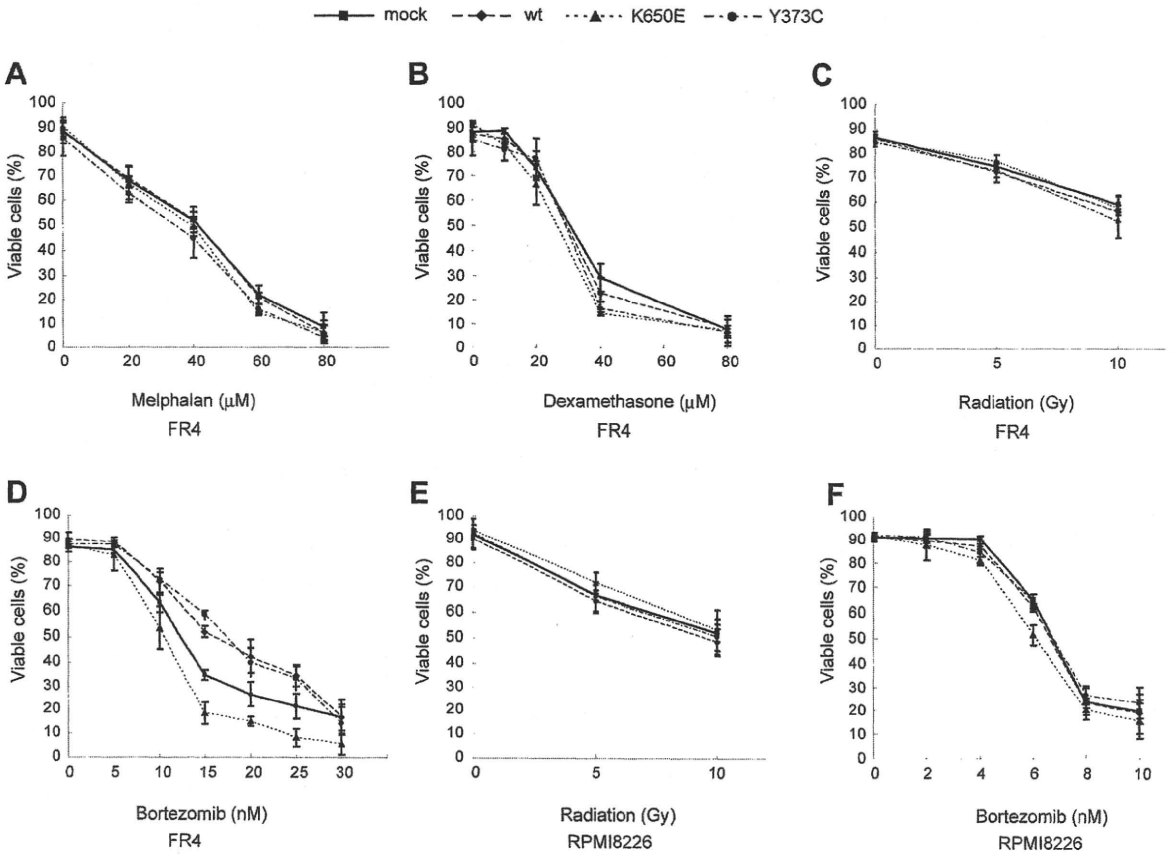

Figure 3. *Treatment of FGFR3-transduced cells with melphalan, dexamethasone and bortezomib. A, B and D: Mock, wild-type (wt), K650E and Y373C FR4 cells were incubated with various drug concentrations and analysed using Annexin V assay kit 48 hours after induction. C: FR4 cells were irradiated with 5 or 10 Gy. E and F: Mock, wt, K650E and Y373C RPMI8226 cells were treated with irradiation (E) or bortezomib (F). Increased apoptosis was observed in K650E FR4 cells and K650E RPMI8226 cells after treatment with bortezomib.*

highest in KE-FR4 cells. CHOP, a mediator of apoptosis induced by ER stress, was strongly induced by bortezomib in all cell lines, the magnitude of which was significantly increased in FR4-KE cells (Figure 4A-D). Immunoblotting of cell lysates in similar conditions demonstrated an increase of CHOP expression, particularly in KE-transfected cells. These results indicated that high level of bortezomib-induced ER stress in KE-transfected cells mediate bortezomib efficacy.

Alteration of bortezomib sensitivity by co-treatment with tunicamycin or cycloheximide. This study hypothesized that the difference in bortezomib sensitivity between cell types may be caused by the level of bortezomib-induced ER stress. To confirm this hypothesis, the apoptosis assay was performed after treatment with bortezomib alone or together with the ER stressor, tunicamycin, or the reliever of ER stress, cycloheximide, for 24 hours (Figure 5A, B). Tunicamycin inhibits *N*-linked glycosylation, which results in ER stress (16). Meanwhile, cycloheximide is reported to decrease ER stress by reducing the overall levels of client proteins in the ER (17). The results of this study revealed that the combination of bortezomib and tunicamycin enhanced the cytotoxicity of bortezomib, resulting in the comparable apoptosis in each cell type. In contrast, ameliorating ER stress with cycloheximide reversed the cytotoxic activity of bortezomib, leading to similar survival of each cell type. These results supported the notion that the high sensitivity to bortezomib of malignant plasma cells with $FGFR3^{K650E}$ is mediated by the increased ER stress induced by bortezomib.

Discussion

It has been reported that t(4;14) has poor prognostic value for both the event-free and overall survival in MM patients (18). Recently, patients who expressed FGFR3 responded equally well and had similar outcomes with bortezomib compared

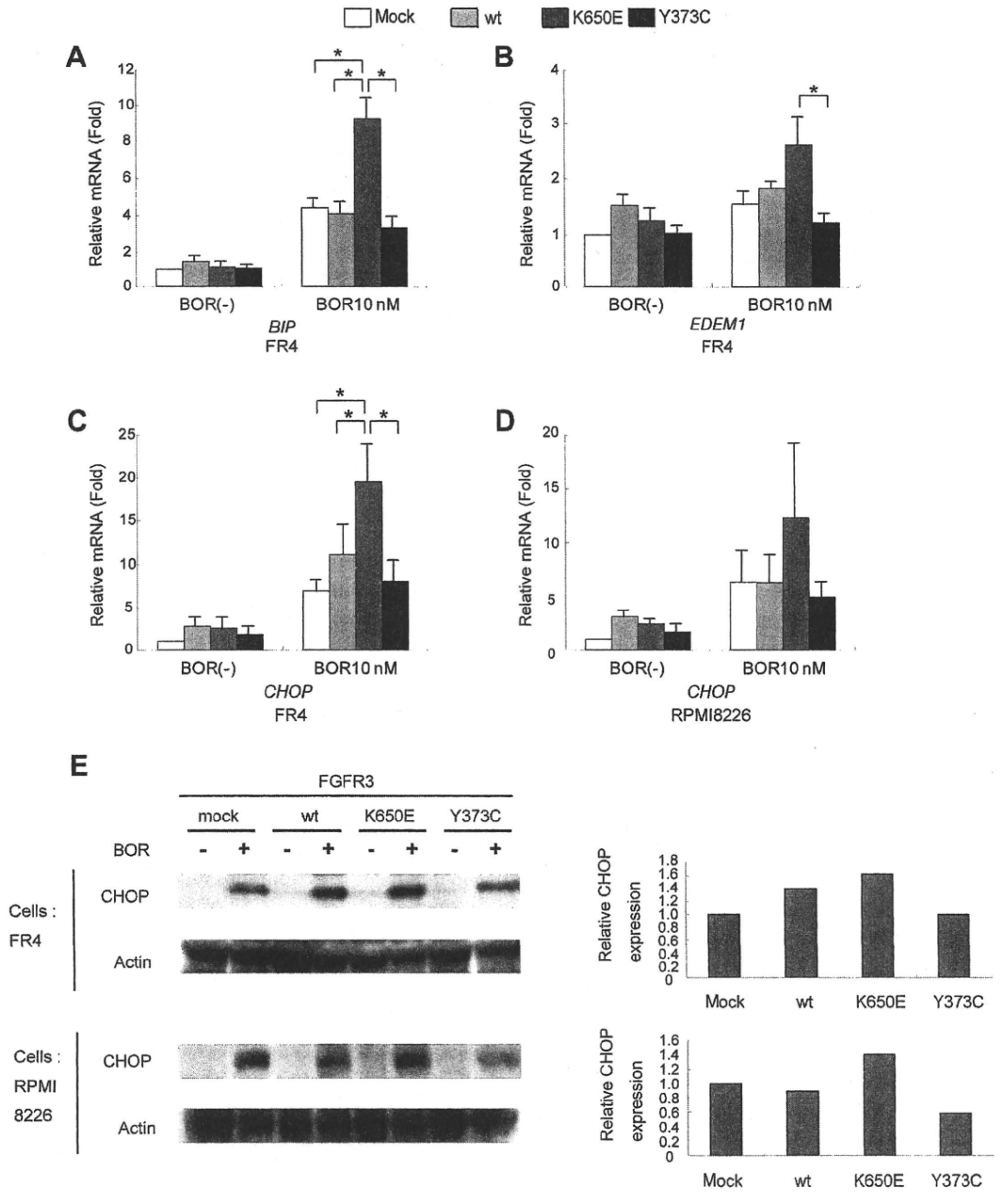

Figure 4. *A-D: Cellular effects of ER stress induced by bortezomib. Transcriptional up-regulation of BIP, EDEM1 and CHOP were observed by real-time PCR. E: Left panel: Up-regulation of CHOP in FR4 and RPMI8226 cells occurred in response to bortezomib. Actin was used as loading control. Right panel: Quantification of CHOP protein in FR4 and RPMI8226 cells treated with bortezomib was performed by image Quant 5.2. The values are given as fold-change relative to the mock cells.*

with FGFR3-negative patients (19). Since it is generally acknowledged that overexpression of receptor tyrosine kinase confers resistance to chemotherapy, these reports support the notion that bortezomib induces apoptosis by a different pathway compared to classical chemotherapeutic drugs. With regard to the constitutive active mutations of *FGFR3*, there are no reports about the efficacy of bortezomib. A few reports indicate that bortezomib is effective on myeloma or lymphoma cells with FGFR3 expression, especially those with constitutively activated K650E mutation and it is related

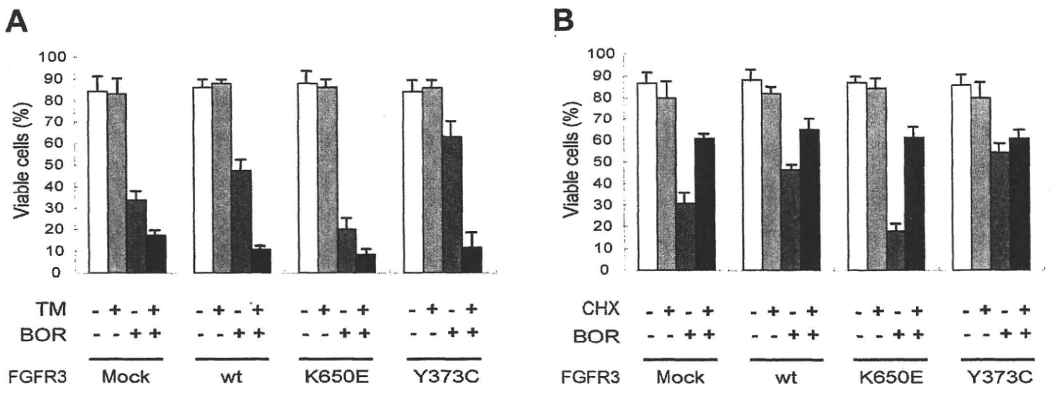

Figure 5. *Accumulation of ER stress with tunicamycin enhanced the cytotoxic effect of bortezomib, whereas amelioration of ER stress with cycloheximide reversed the resistance to bortezomib. A: Viable cells after treatment with bortezomib (10 nM) and tunicamycin (1 μg/ml) for 24 hours. B: Surviving fraction of FR4 cells after treatment with bortezomib (10 nM) and cycloheximide (1 μg/ml) for 24 hours.*

to signal transduction of FGFR3 (20, 21). However, the details of the mechanism are still unclear.

The present study found that myeloma cells with *FGFR3*^{K650E} are sensitive to bortezomib compared with *FGFR3*^{WT}- and *FGFR3*^{Y373C}-transfected cells. In order to understand the relationship between *FGFR3* mutation and bortezomib sensitivity, this study focused on the mechanism by which bortezomib loads ER stress on MM cells. Plasma cells synthesize and secrete large quantities of monoclonal paraprotein. In this process, immunoglobulins are folded into their tertiary structures within the ER, where UPR maintains proper protein folding. If the UPR is unable to maintain protein production, an ER stress signal is generated and apoptosis ensues. From this point of view, the plasma cell tumor is notably vulnerable to ER stress, in the condition that the UPR response is compromised. Proteasome inhibitor is thought to disrupt the unfolded protein response in MM cells and inhibit cells to handle the proper folding of proteins (22). Though the precise mechanism of ER stress-induced apoptosis is still unclear, the proapoptotic protein CHOP is considered to play a significant role in ER-dependent cell death (23). CHOP protein is induced by unfolded protein response and leads cells to apoptosis (24-26). Certainly, in this study, CHOP was induced by bortezomib, especially in cells with K650E mutant. *BIP* and *EDEM1* genes, both of which are known to code for ER stress proteins and are related to ER reticulum-associated degradation (27, 28), were also induced most prominently in cells with K650E by bortezomib treatment. In the combined treatment of bortezomib and tunicamycin, an ER stressor, tunicamycin increased bortezomib-induced cell death, which resulted in comparable levels of apoptosis between cells with K650E and others. In contrast, relieving ER stress by cycloheximide, a translation inhibitor, reversed the enhanced cytotoxic activity of bortezomib in cells with K560E mutant. Taken together, these results indicate that the increased ER stress loaded by bortezomib is closely related to the enhanced apoptosis of KE-FR4 cells.

There are reports which indicate that constitutively active mutant proteins of receptor tyrosine kinase, such as c-Kit^{Asp816Val} or FLT3 internal tandem duplication (ITD), are mainly localized in Golgi or ER as an unglycosylated immature forms (29, 30). A report regarding FLT3-ITD also suggested that the aberrant activation of tyrosine phosphorylation itself impedes the maturation of the receptor tyrosine kinase (31). In addition, FLT3-ITD localized in ER may preferentially activate STAT5, but failed to activate PI3K and MAPK signaling (29). Concerning *FGFR3* mutants, it was reported that constitutively active kinase activity also affects the maturation and trafficking of mutant FGFR (32, 33). Consistent with these reports, immunocytochemical analysis revealed that FGFR3^{K650E} is localized in the ER as a constitutively active form, different from FGFR3^{Y373C} and FGFR3^{WT} also in malignant plasma cells. It is hypothesized that deregulated accumulation of mutant FGFR3 in the ER may be a possible cause for the enhanced ER stress, since the ER localization of K650E mutant is the specific characteristic different from Y373C mutant or wild-type. There are some data about the association between ER stress and the activation of ER-localized tyrosine kinase. ABL tyrosine kinase was reported to be localized in the ER and mediate ER stress-induced apoptosis (34), while another report showed that imatinib, an inhibitor of ABL kinase, ameliorates ER stress and induces remission of diabetes in *db/db* mice (35). It is suggested that the aberrant localization of constitutive active tyrosine kinase in the ER may phosphorylate the ER-resident proteins which imitates the function of ABL kinase, thereby augmenting ER

stress. Another possibility is that the existence of active tyrosine kinase in the ER itself may induce ER stress since, in general, the receptor tyrosine kinase is subject to the degradation after the activation, which requires the disposal at the proteasome. Further studies are necessary for the clarification of the association between enhanced ER stress and ER-localized activation of tyrosine kinase.

This study herein suggested that bortezomib is effective on cells with specific *FGFR3* mutation and the increased cytotoxicity is ER stress-dependent and may be related to the localization of mutant receptor tyrosine kinase. Since mutations of receptor tyrosine kinase are prevalent in neoplastic cells other than hematological malignancy, this study suggests a novel possibility that proteasome inhibitor may work as a specific targeting drug for cancer cells with mutant tyrosine kinases.

Acknowledgements

This work was supported by grants from the Ministry of Education, Culture, Sports, Science and Technology of Japan. The Authors thank Noriko Kikunaga and Yoko Habuchi for their professional assistance; Masato Yasumi, Norimitsu Saitoh, Jun Ishiko, Hirohiko Shibayama, Shinichi Tagawa for their helpful advice and discussion.

References

1 Chesi M, Nardini E, Brents LA, Schröck E, Ried T, Kuehl WM and Bergsagel PL: Frequent translocation t(4;14)(p16.3;q32.3) in multiple myeloma is associated with increased expression and activating mutations of fibroblast growth factor receptor 3. Nat Genet *16*: 260-264, 1997.

2 Chesi M, Brents LA, Ely SA, Bais C, Robbiani DF, Mesri EA, Kuehl WM and Bergsagel PL: Activated fibroblast growth factor receptor 3 is an oncogene that contributes to tumor progression in multiple myeloma. Blood *97*: 729-736, 2001.

3 Plowright EE, Li Z, Bergsagel PL, Chesi M, Barber DL, Branch DR, Hawley RG and Stewart AK: Ectopic expression of fibroblast growth factor receptor 3 promotes myeloma cell proliferation and prevents apoptosis. Blood *95*: 992-998, 2000.

4 Cappellen D,De Oliveira C, Ricol D, de Medina S, Bourdin J, Sastre-Garau X, Chopin D, Thiery JP and Radvanyi F: Frequent activating mutations of *FGFR3* in human bladder and cervix carcinomas. Nat Genet *23*: 18-20, 1999.

5 Ronchetti D, Greco A, Compasso S, Colombo G, Dell'Era P, Otsuki T, Lombardi L and Neri A: Deregulated *FGFR3* mutants in multiple myeloma cell lines with t(4;14): comparative analysis of Y373C, K650E and the novel G384D mutations. Oncogene *20*: 3553-3562, 2001.

6 Barr P, Fisher R and Friedberg J: The role of bortezomib in the treatment of lymphoma. Cancer Invest *25*: 766-775, 2007.

7 Khnykin D, Troen G, Berner JM and Delabie J: The expression of fibroblast growth factors and their receptors in Hodgkin's lymphoma. J Pathol *208*: 431-438, 2006.

8 Maeda T, Yagasaki F, Ishikawa M, Takahashi N and Bessho M: Transforming property of TEL-FGFR3 mediated through PI3-K in a T-cell lymphoma that subsequently progressed to AML. Blood *105*: 2115-2123, 2005.

9 Plotnikov AN, Schlessinger J, Hubbard SR and Mohammadi M: Structural basis for FGF receptor dimerization and activation. Cell *98(5)*: 641-650, 1999.

10 Sibley K, Fenton JA, Dring AM, Ashcroft AJ, Rawstron AC and Morgan GJ: A molecular study of the t(4;14) in multiple myeloma. Br J Haematol *118*: 514-520, 2002.

11 Hideshima T, Chauhan D, Richardson P and Anderson KC: Identification and validation of novel therapeutic targets for multiple myeloma. J Clin Oncol *23*: 6345-6350, 2005.

12 Richardson PG, Mitsiades C, Hideshima T and Anderson KC: Bortezomib: proteasome inhibition as an effective anticancer therapy. Annu Rev Med *57*: 33-47, 2006.

13 Bianchi G, Oliva L, Cascio P, Pengo N, Fontana FCerruti F, Orsi A, Pasqualetto E, Mezgharani A, Calbi V, Palladini G, Giuliani N, Anderson KC, Sitia R and Cenci S: The proteasome load *versus* capacity balance determines apoptotic sensitivity of multiple myeloma cells to proteasome inhibition. Blood *113*: 3040-3049, 2009.

14 Chen J, Williams IR, Lee BH, Duclos N, Huntly BJ, Donoghue DJ and Gilliland DG: Constitutively activated *FGFR3* mutants signal through PLCgamma-dependent and -independent pathways for hematopoietic transformation. Blood *106*: 328-37, 2005.

15 Tagawa S, Doi S, Taniwaki M, Abe T, Kanayama Y, Nojima J, Matsubara K and Kitani T: Amylase-producing plasmacytoma cell lines, AD3 and FR4, with der(14)t(8;14) and dic(8)t(1;8) established from ascites. Leukemia *4*: 600-605, 1990.

16 Helenius A and Aebi M: Roles of *N*-linked glycans in the endoplasmic reticulum. Annu Rev Biochem *73*: 1019-1049,2004

17 Endo H, Murata K, Mukai M, Ishikawa O and Inoue M: Activation of insulin-like growth factor signaling induces apoptotic cell death under prolonged hypoxia by enhancing endoplasmic reticulum stress response. Cancer Res *67*: 8095-8103, 2007

18 Avet-Loiseau H, Attal M, Moreau P, Charbonnel C, Garban F, Hulin C, Leyvraz S, Michallet M, Yakoub-Agha I, Garderet L, Marit G, Michaux L, Voillat L, Renaud M, Grosbois B, Guillerm G, Benboubker L, Monconduit M, Thieblemont C, Casassus P, Caillot D, Stoppa AM, Sotto JJ, Wetterwald M, Dumontet C, Fuzibet JG, Azais I, Dorvaux V, Zandecki M, Bataille R, Minvielle S, Harousseau JL, Facon T and Mathiot C: Genetic abnormalities and survival in multiple myeloma: the experience of the Intergroupe Francophone du Myelome. Blood *109*: 3489-3495, 2007.

19 Dawson MA, Opat SS,Taouk Y, Donovan M, Monaghan K, Horvath N, Roberts AW, Prince HM, Hertzberg M, McLean CA and Spencer A: Clinical and immunohistochemical features associated with a response to bortezomib in patients with multiple myeloma. Clin Cancer Res *15*: 714-722, 2009.

20 Guan M, Zhu L, Somlo G, Hughes A, Zhou B and Yen Y: Bortezomib therapeutic effect is associated with expression of FGFR3 in multiple myeloma cells. Anticancer Res *29*: 1-9, 2009.

21 Zheng W, Guan M, Zhu L, Cai Z, Chung V, Huang H and Yen Y: Bortezomib therapeutic effect is associated with expression and mutation of *FGFR3* in human lymphoma cells. Anticancer Res *30*: 1921-1930, 2010.

22 Lee AH, Iwakoshi NN, Anderson KC and Glimcher LH: Proteasome inhibitors disrupt the unfolded protein response in myeloma cells. Proc Natl Acad Sci USA *100*: 9946-9951, 2003.

23 Song B, Scheuner D, Ron D, Pennathur S and Kaufman RJ: Chop deletion reduces oxidative stress, improves beta cell function, and promotes cell survival in multiple mouse models of diabetes. J Clin Invest *118*: 3378-3389, 2008.

24 Gotoh T and Mori M: Nitric oxide and endoplasmic reticulum stress. Arterioscler Thromb Vasc Biol *26*: 1439-1446, 2006.
25 Novoa I, Zeng H, Harding HP and Ron D: Feedback inhibition of the unfolded protein response by GADD34-mediated dephosphorylation of eIF2alpha. J Cell Biol *153*: 1011-1022, 2001.
26 Novoa I, Zhang Y, Zeng H, Jungreis R, Harding HP and Ron D: Stress-induced gene expression requires programmed recovery from translational repression. EMBO J *22*: 1180-1187, 2003.
27 Hendershot LM: The ER function BIP is a master regulator of ER function. Mt Sinai J Med *71*: 289-297, 2004.
28 Hosokawa N, Wada I, Hasegawa K, Yorihuzi T, Tremblay LO, Herscovics A and Nagata K: A novel ER alpha-mannosidase-like protein accelerates ER-associated degradation. EMBO Rep *2*: 415-422, 2001.
29 Choudhary C, Olsen JV, Brandts C, Cox J, Reddy PN, Böhmer FD, Gerke V, Schmidt-Arras DE, Berdel WE, Müller-Tidow C, Mann M and Serve H: Mislocalized activation of oncogenic RTKs switches downstream signaling outcomes. Mol Cell *36*: 326-339, 2009.
30 Xiang Z, Kreisel F, Cain J, Colson A and Tomasson MH: Neoplasia driven by mutant c-KIT is mediated by intracellular, not plasma membrane, receptor signaling. Mol Cell Biol *27*: 267-282, 2007.
31 Schmidt-Arras DE, Böhmer A, Markova B, Choudhary C, Serve H and Böhmer FD: Tyrosine phosphorylation regulates maturation of receptor tyrosine kinases. Mol Cell Biol *25*: 3690-3703, 2005.
32 Lievens PM and Liboi E: The thanatophoric dysplasia type II mutation hampers complete maturation of fibroblast growth factor receptor 3 (FGFR3), which activates signal transducer and activator of transcription 1 (STAT1) from the endoplasmic reticulum. J Biol Chem *278*: 17344-17349, 2003.
33 Lievens PM, Mutinelli C, Baynes D and Liboi E: The kinase activity of fibroblast growth factor receptor 3 with activation loop mutations affects receptor trafficking and signaling. J Biol Chem *279*: 43254-43260, 2004.
34 Qi X and Mochly-Rosen D: The PKCdelta -Abl complex communicates ER stress to the mitochondria – an essential step in subsequent apoptosis. J Cell Sci *121*: 804-813, 2008.
35 Han MS, Chung KW, Cheon HG, Rhee SD, Yoon CH, Lee MK, Kim KW and Lee MS: Imatinib mesylate reduces endoplasmic reticulum stress and induces remission of diabetes in *db/db* mice. Diabetes *58*: 329-336, 2009.

Received November 13, 2010
Revised December 6, 2010
Accepted December 6, 2010

INTERNAL MEDICINE

□ CASE REPORT □

Pulmonary Arterial Hypertension Associated with Chronic Active Epstein-Barr Virus Infection

Takahiro Hashimoto[1], Yasushi Sakata[1], Kentaro Fukushima[2], Tetsuo Maeda[2], Yoh Arita[1], Wataru Shioyama[1], Yoshikazu Nakaoka[1], Yumiko Hori[3], Eiichi Morii[3], Katsuyuki Aozasa[3], Yuzuru Kanakura[2], Keiko Yamauchi-Takihara[1] and Issei Komuro[1]

Abstract

A 45-year-old man with chronic active Epstein-Barr virus (EBV) infection (CAEBV) with natural killer cell type developed pulmonary arterial hypertension (PAH). After chemotherapy, he showed marked depression of the EBV DNA genome in the peripheral blood, but PAH sustained. He died of heart failure due to PAH, and the histo-pathological examination revealed pulmonary vascular abnormalities without lung disease on autopsy. Although the EBV DNA genome and the infiltrating lymphocytes were not detected in the lung, his clinical course suggested that his PAH might be caused by CAEBV. This is the first reported case of PAH associated CAEBV in an adult.

Key words: Epstein-Barr virus, pulmonary arterial hypertension, inflammation, right heart failure

(Intern Med 50: 119-124, 2011)
(DOI: 10.2169/internalmedicine.50.4143)

Introduction

Epstein-Barr virus (EBV) is a ubiquitous virus in humans, and most individuals are infected by early adulthood. The primary infection of EBV is usually asymptomatic, and EBV has been latent in B cells for life in the normal host after primary infection. Symptomatic acute EBV infection is clinically recognized as infectious mononucleosis (IM), which basically follows a self-limited course due to the integrated cellular immune response. The clinical manifestations seen in IM are the consequence of cytotoxic T lymphocyte response against polyclonal proliferation of EBV-infected B cells. However, some individuals in Asia are reported to develop chronic infection with EBV. Chronic active EBV infection (CAEBV) is characterized by chronic recurrent infectious mononucleosis-like symptoms over a long period of time and by an unusual pattern of anti-EBV-antibodies (1-6). CAEBV is a disease with a high mortality with life-threatening complications, such as virus-associated hemophagocytic syndrome, EBV-positive lymphoid neoplasia mainly in T-cell and natural killer (NK) cell lineage, interstitial pneumonia, cardiovascular diseases and large-vessel arteritis with infiltration of EBV-positive lymphoid cells (7-18).

Approximately one-fourth of CAEBV patients develop inflammatory vascular lesions. Affinity of EBV-infected lymphoid cells to large vessels involving coronary arteries, aorta, and its major branches has been reported, but not in small vessels (12-18). In this report, we describe occlusive vasculopathy of the small pulmonary arteries and arterioles in a patient with CAEBV associated with pulmonary arterial hypertension (PAH).

Case Report

A previously healthy, 41-year-old Japanese man was initially seen with abnormal liver function by annual medical examination in June 2006. His family history was unremarkable and he had been smoking since he was 20 years old, with Brinkman index of 400. Since July 2007, he exhibited thrombocytopenia, splenomegaly and liver dysfunction (Ta-

[1]Department of Cardiovascular Medicine, Osaka University Graduate School of Medicine, Japan, [2]Department of Hematology and Oncology, Osaka University Graduate School of Medicine, Japan and [3]Department of Pathology, Osaka University Graduate School of Medicine, Japan
Received for publication June 29, 2010; Accepted for publication September 27, 2010
Correspondence to Dr. Keiko Yamauchi-Takihara, takihara@imed3.med.osaka-u.ac.jp

Table 1. Changes in Clinical Parameters

	2006. 6	2007. 7	2009. 1	2009. 2	2009. 4	2009. 7	2009. 8
AST (IU/L)	59	72	147	104	121	29	29
ALT (IU/L)	50	83	88	88	76	29	23
PLT ($\times 10^4/\mu L$)	N/A	11.4	6.6	5.1	4.2	8.6	11.4
Proteinuria (g/day)	(-)	(-)	3.5	3.6	0.7	N/A	0.1
CRP (mg/dL)	N/A	N/A	0.17	0.25	0.19	0.42	0.30
EBV DNA (copy/ml in plasma)	N/A	N/A	N/A	N/A	2000	200	200
NYHA class	I	I	II	II	II	II	III
6MWD (m)	N/A	N/A	N/A	440	N/A	400	N/A
BNP (pg/mL)	N/A	N/A	543	238	243	219	141
UA (mg/dL)	N/A	5.8	9.2	4.8	8.7	7.6	8.7
TR-PG (mmHg)	N/A	N/A	97	121	127	100	132

AST: aspartate aminotransferase, ALT: alanine aminotransferase, PLT: platelets, CRP: C-reactive protein, EBV: Epstein-Barr virus infection,
NYHA: New York Heart Association functional class, 6MWD: 6-minute walking distance, BNP: brain natriuretic peptide, UA: uric acid, TR-PG: tricuspid regurgitation-pressure gradient, N/A: not available.
The 6MWD test was performed according to modified American Thoracic Society standards.

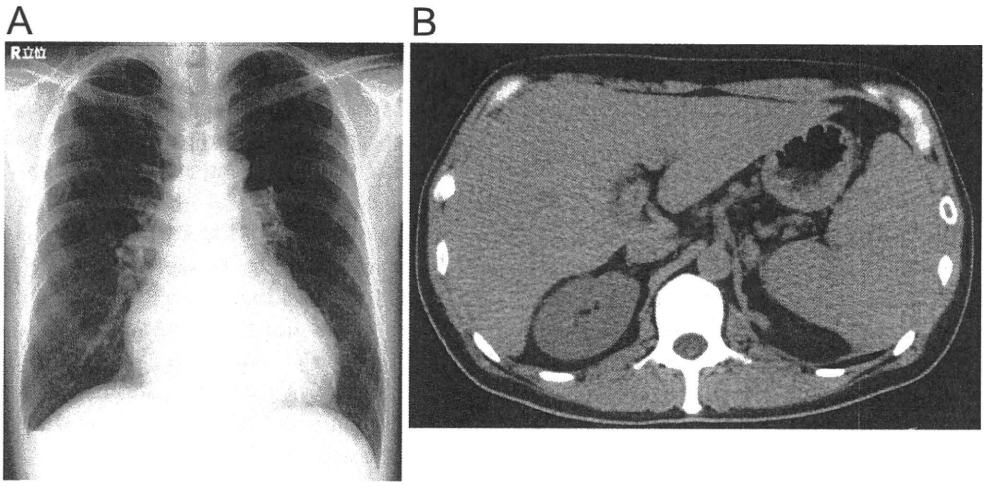

Figure 1. Chest radiography (A) and abdominal computed tomography (B) of January 2009.

ble 1).

He gradually developed dyspnea of New York Heart Association (NYHA) class II, and was admitted to Osaka Saiseikai Senri Hospital with systemic edema in January 2009. Laboratory examination showed thrombocytopenia, liver dysfunction, hypoproteinemia, and proteinuria (Table 1). Brain natriuretic peptide (BNP) was 543 pg/mL and oxygen saturation was 93% on room air. Chest radiography revealed pulmonary artery dilation, pleural effusion, and cardiomegaly (CTR: 59%) (Fig. 1A). Electrocardiogram (ECG) showed sinus tachycardia of 102 bpm and right ventricular hypertrophy. Echocardiographic (UCG) examination showed normal left ventricular contraction and tricuspid regurgitation-pressure gradient (TR-PG) was 97 mmHg, and reverse curvature of the inter-ventricular septum was noted at that time. He was clinically diagnosed with pulmonary hypertension and nephrotic syndrome. Chest computed tomography (CT) and lung perfusion scintigraphy yielded no evidence of pulmonary thromboembolism, and enhanced CT revealed no pulmonary embolism. Spirometry resulted with

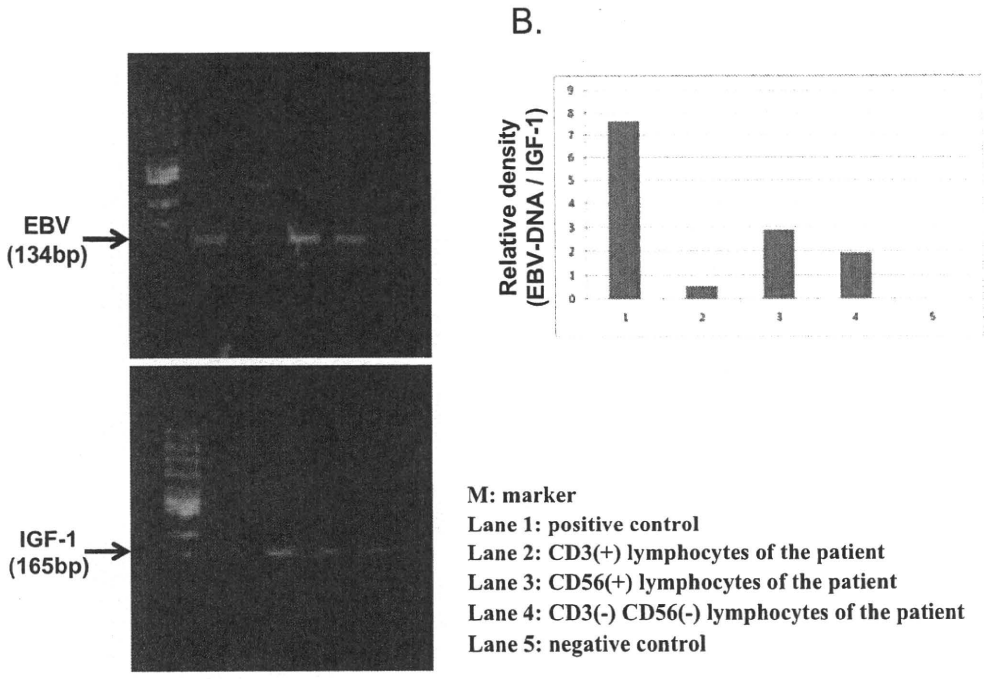

Figure 2. Quantitative polymerase chain reaction (PCR) analysis for the Epstein-Barr virus (EBV) genome. A: DNA was extracted by using QIAamp DNA Mini Kit® (Qiagen, Hilden, Germany) from peripheral blood lymphocytes obtained by EasySep® (Stem Cell Technologies). EBV genome was amplified by using following primers with expected length of DNA 134 bps; S: 5′-CAAGAACCCAGACGAGTCCGTAGAA-3′, AS: 5′-AAGAAGCATGTATACTAAGCCTCCC-3′. Insulin-like growth factor-1 (IGF-1) was applied as an internal control by using following primers (expected length:165 bps); S: 5′-AGAGTGGTGGGGTGGGGAGGG-3′, AS: 5′-GGGCAGGCAGCATTGGATTGG-3′. DNA from the patient who was previously diagnosed as CAEBV was used as a positive control (lane 1). The solution without DNA was used as a negative control (lane 5). B: The amount of EBV-DNA was estimated by the ratio of EBV-DNA to IGF-1 obtained from each cell subset.

normal pulmonary function. Abdominal CT revealed hepatosplenomegaly (Fig. 1B). The results of right heart catheterization (RHC) were as follows; the mean pulmonary artery pressure (mPAP) 64 mmHg, pulmonary capillary wedge pressure (PCWP) 9 mmHg, mean right atrial pressure (RAP) 5 mmHg, cardiac index (CI) 2.54 L/min/m^2, and pulmonary vascular resistance 1,062 dyne·sec/cm^5.

He was treated with candesartan cilexetil and diuretics, and his general condition was improved. After two weeks of treatment, six-minute walking distance (6MWD) test was 440 m and BNP and uric acid decreased to 238 pg/mL and 4.8 mg/dL, respectively (Table 1).

He was transferred to National Cardiovascular Center for the further examination of hepatosplenomegaly in February 2009. On admission, atypical lymphocytes were detected in the peripheral blood and Epstein-Barr virus-related antibody titers were as follows; anti-VCA IgG 1,280× IgM <10×, anti-EA IgG 40×, and anti-EBV nuclear antigens (EBNA) < 10×. The EBV genome ($10^{5.7}$ copies/μg DNA) was clearly detected in the peripheral blood by polymerase chain reaction analysis. As shown in Fig. 2, EBV was highly detected in CD56 (+) lymphocytes, but not in CD3 (+) lymphocytes. These results suggest that EBV-infected mononuclear cells were NK cells. As other possible diseases, such as collagen disease, were denied based on the clinical and laboratory findings, he was diagnosed as a CAEBV with NK-cell type.

For the further treatment of CAEBV, he was transferred to the Department of Hematology and Oncology, Osaka University Hospital in early April 2009. Arterial blood gas analysis was a PaO_2 of 68.9 mmHg and a $PaCO_2$ of 34.9 mmHg on room air. Bone marrow aspiration revealed absence of hemophagocytosis. The monoclonal proliferation of EBV-infected cells was detected from a bone marrow specimen by Southern blot analysis.

The immunochemotherapy; 50 mg prednisolone, 200 mg/day cyclosporine for 10 days, and 225 mg etoposide, in accordance with HLH-2004 protocol, was started from mid-April (19). At the end of April he developed continuous high fever, and Listeria meningoencephalitis was diagnosed by lumbar puncture and brain magnetic resonance imaging. This was identified as a side-effect caused by immunosuppressive drugs, therefore, the therapy was abandoned due to a side-effect on the following day. The antimicrobial combination of sulfamethoxazole/trimethoprim and doripenem and

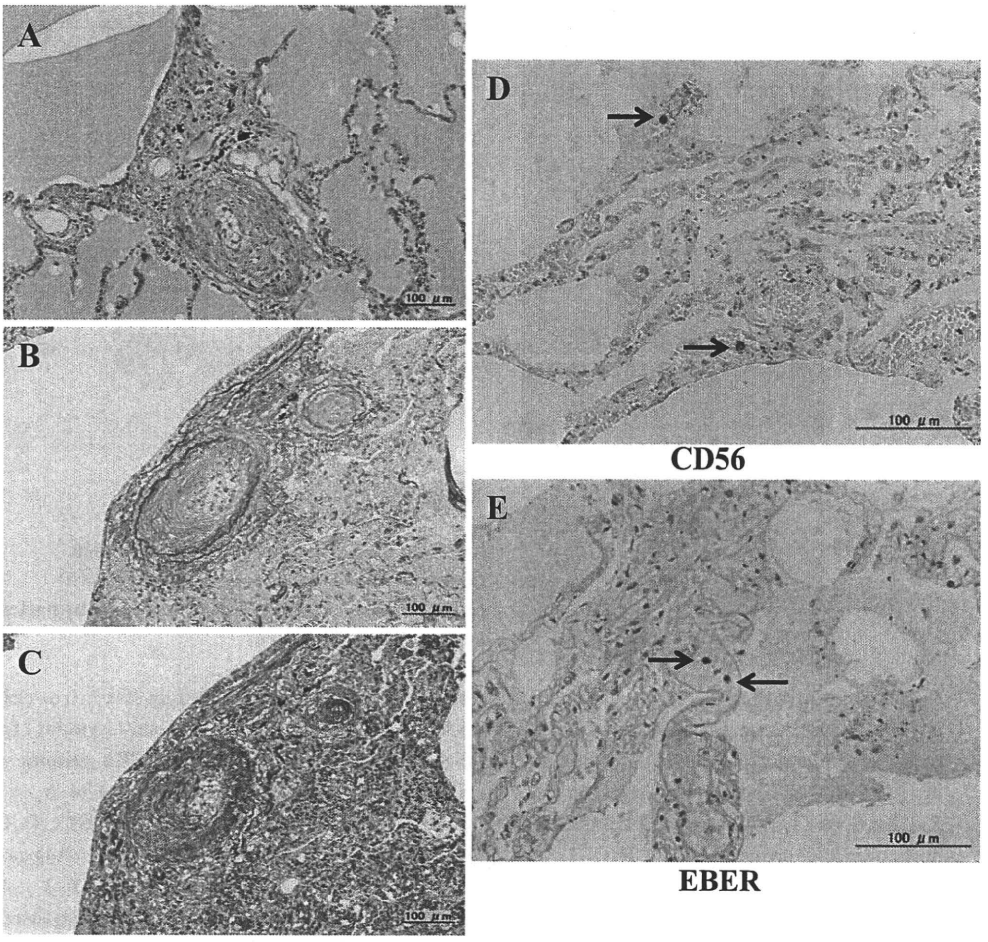

Figure 3. Pathological examination of pulmonary arterial lesions. Panel A (Hematoxylin and Eosin staining) and B (Elastica van Gieson): Concentric intimal cellular proliferation with marked luminal narrowing. Panel C (Azan): Intimal fibrosis is stained blue. Panel D: CD56 staining. CD56-positive cells are observed within the small vascular spaces (Arrows). Panel E: in situ hybridization of EBV-encoded small ribonucleic acid (EBER). EBER-positive lymphocytes are observed within the small vascular spaces (Arrows), but not in the arteriolar wall. Original magnification ×100 in A, B and C, ×200 in D and E.

tobramycin was effective for the treatment of Listeria meningoencephalitis. Although the immunochemotherapy improved liver dysfunction and reduced the amount of EBV DNA in plasma, disorientation and memory impairment were left as after effects of meningoencephalitis. His general condition remained in NYHA Class II, and he left the hospital in early August 2009 with home oxygen therapy.

He was re-hospitalized in the Department of Cardiovascular Medicine, Osaka University Hospital in mid-August 2009 with symptoms of severe heart failure of NYHA Class III. On admission, his heart rate was 86 bpm, his blood pressure was 84/70 mmHg, and oxygen saturation was 93% with 3 L/min nasal O_2. TR-PG was 132 mmHg by UCG, and RHC resulted mPAP 61 mmHg, mean RAP 5 mmHg, and CI 2.02 L/min/m^2.

Furosemide, dobutamine and olprinone hydrochloride hydrate were started for the treatment of heart failure. Additionally, warfarin and sildenafil (40 mg/day) were started. Epoprostenol sodium (0.25 ng/kg/min) was started from the end of August, gradually increased to 3.0 ng/kg/min, and subsequently he had slight improvement. In mid-September, he developed a prostatic abscess accompanied by high fever, and his condition rapidly worsened. On the same day, he suddenly died and an autopsy was performed. The cause of his death was diagnosed as acute circulatory failure due to severe PAH, which was exaggerated by high fever.

Pathological findings

The predominant finding of the lung was plexogenic pulmonary arteriopathy and the heart showed RV dilatation and hypertrophy. Histological examination of the lung revealed adventitial fibrosis, marked concentric and eccentric laminar intimal proliferation, mild medial hypertrophy, and occlusion of pulmonary arteries mainly in small arteries with 200-300 μm in diameter (Fig. 3A, B, C). It was notable that intimal thickening was more marked than that in media. Pulmonary

abnormality was not shown except for bilateral slight emphysematous changes in apical portions of the lung. There was no thrombotic lesion. These findings were compatible with PAH, and the vascular diseases were classified as Grade 3 of the Heath-Edwards grading system.

Immunohistochemical examination showed that EBV- encoded small ribonucleic acid (EBER)-positive cells and CD 56-positive cells were present within the small vascular spaces, but no infiltration of EBER-positive lymphocytes was observed in the diseased arteriolar wall (Fig. 3D, E). There was no evidence of left heart disease including myocarditis and coronary aneurysm.

Discussion

The autopsy case of CAEBV described herein was complicated by plexogenic pulmonary arteriopathy. Both CAEBV and PAH are very rare disorders, therefore it is quite unlikely that they developed independently at the same time. Furthermore, heart failure developed one year from the onset of CAEBV, which suggest that PAH might be caused by CAEBV.

Cardiovascular complications are not rare in patients with CAEBV. There are some reported cases of CAEBV in association with aneurysm of the coronary artery and aorta. In these cases the aneurysm showed marked intimal fibrous thickening, and lymphocytic infiltration were observed around the damaged coronary artery or the vasa vasorum of the diseased arteries (12, 18, 20). In the present case, similar marked intimal fibrous thickening was seen in the pulmonary artery, but there was no EBV-positive NK cells infiltrated into the vessel wall. There is a possibility that immunochemotherapy suppressed the inflammation which resulted in the reduction of arteritis at the autopsy.

Previously, Palevsky et al (21) evaluated the vascular structure qualitatively from the specimens of 19 patients with primary pulmonary hypertension. Three components of the vessel were assessed separately: the lumen, the intima, and the media. They showed that the media was more consistently enlarged than the intima in these patients. However, in the present case, intimal proliferation of the pulmonary artery was more marked than in most of the cases with primary pulmonary hypertension. The pathogenesis of arteriopathy complicated with CAEBV, especially the role of EBV-infected lymphocytes, is still unclear. There is similarity between histological findings in this case and those previously reported cardiovascular complications associated with CAEBV. An initial target of arteriopathy was thought to be the intima of a small vessel less than 500 μm such as vasa vasorum or arteriole.

There are two possible pathological mechanisms that CAEBV causes PAH, one is that EBV caused pulmonary arteritis which results in the structural remodeling of the pulmonary artery, and the other is that chronic infection of EBV induced high levels of inflammatory cytokines that cause inflammatory change in pulmonary artery. Recently, it has been suggested that proinflammatory cytokines may be related to the pathogenesis of pulmonary hypertension (22). In the present case, serum IL-6 concentration was 4.6 pg/mL, which was markedly higher than normal individuals (1.69 ± 0.76 pg/mL, n=162). Inflammatory cytokines released from infiltrating cells might cause endothelial cell dysfunction that results in PAH. The histological findings of diseased artery in this case were different to those of Kawasaki disease, Takayasu arteritis and PAH associated with human immunodeficiency virus.

Although there are reports of child cases of pulmonary hypertension associated with CAEBV, whose pulmonary lesion was presumed as a complication of interstitial pneumonitis, systemic lupus erythematosus and left heart disease, this is the first reported case of PAH associated with CAEBV in an adult. If cardiomegaly or heart failure develop in the course of CAEBV, the possibility of PAH needs to be examined.

The authors state that they have no Conflict of Interest (COI).

References

1. Rickinson AB. Chronic, symptomatic Epstein-Barr virus infection. Immunol Today **7**: 13-14, 1986.
2. Straus SE. The chronic mononucleosis syndrome. J Infect Dis **157**: 405-412, 1988.
3. Rickinson AB, Kieff E. Epstein-Barr virus. In: Virology. Vol. 2. Fields BN, Knipe DM, Howly PM, Eds. Lippincott-Raven, Philadelphia, PA, 1996: 2397-2446.
4. Cohen JI. Epstein-Barr virus infection. N Engl J Med **343**: 481-492, 2000.
5. Kimura H, Hoshino Y, Kanegane H, et al. Clinical and virologic characteristics of chronic active Epstein-Barr virus infection. Blood **98**: 280-286, 2001.
6. Kasahara Y, Yachie A, Takei K, et al. Differential cellular targets of Epstein-Barr virus (EBV) infection between acute EBV-associated hemophagocytic lymphohistiocytesis and chronic active EBV infection. Blood **98**: 1882-1888, 2001.
7. Schooley RT, Carey RW, Miller G, et al. Chronic Epstein-Barr virus infection associated with fever and interstitial pneumonitis. Clinical and serologic features and response to antiviral chemotherapy. Ann Intern Med **104**: 636-643, 1986.
8. Jones J, Shurin S, Abramowsky C, et al. T-cell lymphomas containing Epstein-Barr viral DNA in patients with chronic Epstein-Barr virus infections. N Engl J Med **318**: 733-741, 1988.
9. Kikuta H, Taguchi Y, Tomizawa K, et al. Epstein-Barr virus genome-positive T lymphocytes in a boy with chronic active EBV infection associated with Kawasaki-like disease. Nature **333**: 455-457, 1988.
10. Okano M, Matsumoto S, Osato T, Sakiyama Y, Thiele GM, Purtilo DT. Severe chronic active Epstein-Barr virus infection syndrome. Clin Microbiol Rev **4**: 129-135, 1991.
11. Ohga S, Takada H, Honda K, et al. Central nervous system T-cell lymphoproliferative disorder in a patient with chronic active Epstein-Barr virus infection. J Pediat Hematol Onc **21**: 42-46, 1999.
12. Nakagawa A, Ito M, Iwaki T, Yatabe Y, Asai J, Hayashi K. Chronic active Epstein-Barr virus infection with giant coronary aneurysms. Am J Clin Pathol **105**: 733-736, 1996.
13. Murakami K, Ohsawa M, Hu S-X, Kanno H, Aozasa K, Nose M. Large-vessel arteritis associated with chronic active Epstein-Barr

virus infection. Arthritis Rheum **41**: 369-373, 1998.

14. Loeffel S, Chang C-H, Heyn R, et al. Necrotizing lymphoid vasculitis in X-linked lymphoproliferative syndrome. Arch Pathol Lab Med **109**: 546-550, 1985.

15. Ilowite NT, Flingner CL, Ochs HD, et al. Pulmonary angiitis with atypical lymphoreticular infiltrates in Wiskott-Aldrich syndrome: possible relationship of lymphomatoid granulomatosis and EBV infection. Clin Immunol Immunopathol **41**: 479-484, 1986.

16. Ishihara S, Kawa-Ha K, Okada S, et al. Clinical and epidemiological characteristics of chronic active EB virus infection in Japan. J Jpn Pediatr Soc **95**: 80-90, 1991.

17. Kikuta H, Sakiyama Y, Matsumoto S, et al. Detection of Epstein-Barr virus DNA in cardiac and aortic tissues from chronic, active Epstein-Barr virus infection associated with Kawasaki disease-like coronary artery aneurysms. J Pediatr **123**: 90-92, 1993.

18. Takahashi R, Nishiuchi R, Yasui M, et al. An unusual case of chronic active Epstein-Barr virus infection with coronary arteritis. J Jpn Pediatr Soc **92**: 2185-2192, 1988.

19. Kawa K, Sawada A, Sato M, et al. Excellent outcome of allogeneic hematopoietic SCT with reduced-intensity conditioning for the treatment of chronic active EBV infection. Bone Marrow Transplant 2010 [Epub ahead of print].

20. Murakami K, Ohsawa M, Shu-Xin Hu, et al. Large-vessel arteritis associated with chronic active Epstein-Barr virus infection. Arthritis Rheum **41**: 369-373, 1998.

21. Palevsky HI, Schloo BL, Pietra GG, et al. Primary pulmonary hypertension. Vascular structure, morphometry, and responsiveness to vasodilator agents. Circulation **80**: 1207-1221, 1989.

22. Humbert M, Monti G, Brenot F, et al. Increased interleukin-1 and interleukin-6 serum concentrations in severe primary pulmonary hypertension. Am J Respir Crit Care **151**: 1628-1631, 1995.

Immunology Letters 136 (2011) 61–73

Contents lists available at ScienceDirect

Immunology Letters

journal homepage: www.elsevier.com/locate/immlet

Myeloid neoplasm-related gene abnormalities differentially affect dendritic cell differentiation from murine hematopoietic stem/progenitor cells

Jiro Fujita, Masao Mizuki*, Masayasu Otsuka, Sachiko Ezoe, Hirokazu Tanaka, Yusuke Satoh, Kentaro Fukushima, Masahiro Tokunaga, Itaru Matsumura, Yuzuru Kanakura

Department of Hematology and Oncology, Osaka University Graduate School of Medicine, 2-2, Yamadaoka, Suita, Osaka 565-0871, Japan

ARTICLE INFO

Article history:
Received 7 June 2010
Received in revised form 6 December 2010
Accepted 22 December 2010
Available online 13 January 2011

Keywords:
DC culture
Leukemia
Myelodysplastic syndrome
Tyrosine kinase
Transcription factor
Tumor immunology

ABSTRACT

Dendritic cells (DCs) play important roles in tumor immunology. Leukemic cells in patients with myeloid neoplasms can differentiate into DCs *in vivo* (referred to as *in vivo* leukemic DCs), which are postulated to affect anti-leukemia immune responses. We established a reproducible culture system of *in vitro* FLT3 ligand-mediated DC (FL-DC) differentiation from murine lineage$^-$ Sca-1$^+$ c-Kit^{high} cells (LSKs), which made it possible to analyse the effects of target genes on steady-state DC differentiation from hematopoietic stem/progenitor cells. Using this system, we analysed the effects of various myeloid neoplasm-related gene abnormalities, termed class I and class II mutations, on FL-DC differentiation from LSKs. All class II mutations uniformly impaired FL-DC differentiation maintaining a plasmacytoid DC (pDC)/conventional DC (cDC) ratio comparable to the control cells. In contrast, class I mutations differentially affected FL-DC differentiation from LSKs. FLT3-ITD and a constitutively active form of Ras (CA-N-Ras) yielded more FL-DCs than the control, whereas the other class I mutations tested yielded less FL-DCs. Both FLT3-ITD and FLT3-tyrosine kinase domain (TKD) mutation showed a comparable pDC/cDC ratio as the control. CA-N-Ras, c-Kit-TKD, TEL/PDGFRβ, and FIP1L1/PDGFRα showed a severe decrease in the pDC/cDC ratio. CA-STAT5 and CA-MEK1 severely inhibited pDC differentiation. FLT3-ITD, CA-N-Ras, and TEL/PDGFRβ aberrantly induced programmed death ligand-1 (PD-L1)-expressing DCs. In conclusion, we have established a simple, efficient, and reproducible *in vitro* FL-DC differentiation system from LSKs. This system could uncover novel findings on how myeloid neoplasm-related gene abnormalities differentially affect FL-DC differentiation from murine hematopoietic stem/progenitor cells in a gene-specific manner.

1. Introduction

DCs are professional antigen-presenting cells, and are the only cell type that can prime naive T cells. Hence, DCs play a pivotal role in innate and adaptive immunities as well as tolerance [1,2]. There are at least two major subsets of DCs, cDCs and pDCs [3]. cDCs possess numerous dendrites and exhibit high expression of major histocompatibility complex class II (MHC II), thereby enabling the stimulation of naïve T cells in the presence of appropriate costimulation. By contrast, pDCs have no or few dendrites and exhibit a plasmacytoid round morphology and low expression of MHC II and costimulatory molecules. Therefore, pDCs are poor stimulators of naïve T cells.

In tumor immunology, deregulation of differentiation, maturation, and function of DCs is thought to contribute to the inhibition of anti-tumor immunity, thereby facilitating disease progression [4–6]. DCs in cancer tissue and cancer-draining lymph nodes often display an immature phenotype both in tumor-bearing animals and in patients with cancer [5–7]. These immature DCs are reported to often induce tolerance by presenting antigens to T cells [2,5,8]. Moreover, the immunosuppressive milieu created by tumors frequently causes a decrease in the numbers of cDCs with no or little effect on the numbers of pDCs, which are known to play important roles in the maintenance of tolerance [6,7]. It has also been shown in mouse models that tumors themselves produced tumor-specific tolerance by pDCs or cDCs through expression of indoleamine 2,3-dioxygenase (IDO) or PD-L1 (also called B7-H1), respectively [9,10]. Thus, DC abnormalities in malignant tumors are characterised by the deregulation of the maturation states, subsets, or functions of DCs.

In contrast to non-hematopoietic malignancies, leukemic cells from patients with acute myeloid leukemia (AML) can differentiate into DCs *ex vivo* in the presence of granulocyte macrophage colony-stimulating factor (GM-CSF) with or without interleukin (IL)-4 [11]. These cells retain leukemic gene abnormalities of the original leukemic cells, hence enabling presentation of known and potentially unknown leukemia-associated antigens (LAAs) [12]. Therefore, in the case of AML, leukemia-derived DCs *ex vivo* (*ex*

* Corresponding author. Tel.: +81 6 6879 3871; fax: +81 6 6879 3879.
E-mail address: mizuki@bldon.med.osaka-u.ac.jp (M. Mizuki).

0165-2478/$ – see front matter © 2011 Elsevier B.V. All rights reserved.
doi:10.1016/j.imlet.2010.12.006

vivo leukemic DCs), which are sometimes referred to as AML-DCs or AML-derived DCs, have been used in DC immunotherapy. In addition to *ex vivo* leukemic DCs, populations of spontaneously differentiated DCs *in vivo* from leukemic cells (*in vivo* leukemic DCs) exist in patients with AML [13,14], chronic myeloid leukemia (CML) [15], and myelodysplastic syndrome (MDS) [16,17]. Because DCs derived from normal cells *in vivo* (*in vivo* normal-origin DCs) are present in these patients, one must discriminate the three different types of DCs that may be present in cases of hematopoietic neoplasm: *in vivo* leukemic DCs, *in vivo* normal-origin DCs, and *ex vivo* leukemic DCs. Although *in vivo* leukemic DCs are thought to have LAAs [13,14] and postulated to affect anti-leukemia immune responses, there have been few reports detailing concise examinations about their subsets, maturation state, or function [13–17].

By contrast, much work has been done on *ex vivo* leukemic DCs [11,18], which are cultured in the presence of GM-CSF. However, the concentration of GM-CSF under steady-state conditions is low or undetectable and *in vitro* GM-CSF-mediated DCs (GM-DCs) are regarded as monocyte-derived DCs, which are induced only under *in vivo* inflammatory states [3,19]. By contrast, the FLT3 ligand (FL) is a crucial cytokine for steady-state DC development *in vivo*, and *in vitro* FL-mediated DCs (FL-DCs) are close equivalents to *in vivo* steady-state splenic DCs [3,19,20]. In patients with leukemia, steady-state conditions refer to the early phase of the disease or the phase of minimal residual disease after therapy. Therefore, it is important to examine the properties of *in vivo* leukemic DCs under steady-state conditions, which are postulated to affect host immune responses in a LAA-specific manner. In this study, we aimed to establish a culture method to induce FL-DCs from LSKs, which are the target for leukemic transformation. We selected FL as a cytokine to induce DCs *in vitro*, which is in contrast to previous studies that have used GM-CSF. This system enabled us to evaluate the direct effects of myeloid neoplasm-related gene abnormalities on FL-DC subsets, their maturation state, and function. Our results reveal novel functions of myeloid neoplasm-related gene abnormalities as direct immune modifiers.

2. Materials and methods

2.1. Mice

C57BL/6 mice (6–9 weeks of age) were used for DC cultures. BALB/c mice (10–13 weeks of age) were used for the mixed leukocyte reaction. All animals were maintained in a pathogen-free barrier facility and handled according to institutional guidelines.

2.2. Antibodies and flow cytometry

Single-cell suspensions were treated with an Fc receptor-blocking antibody (2.4G2, BD Biosciences, San Jose, CA). When Fc receptor blocking was inadequate, purified isotype control antibodies were added to 2.4G2. Cells were subsequently stained with monoclonal antibodies conjugated with fluorescein isothiocyanate (FITC), phycoerythrin (PE), allophycocyanin (APC) or phycoerythrin-Cy7 (PE-Cy7). Biotinylated antibodies were detected using FITC conjugated streptavidin. The following antibodies were purchased from BD Biosciences. Gr-1 (RB6-8C5), Mac-1 (M1/70), Ter119 (TER-119), CD3ε (145-2C11), B220 (RA3-6B2), CD11c (HL3), I-A^b (AF6-120.1), CD40 (3/23), CD80 (16-10A1), CD86 (GL1), NK1.1 (PK136), CD172a (Sirp-α, P84), biotin CD24 (M1/69), c-Kit (2B8), Sca-1 (Ly6A/E, D7). The antibodies specific for PDCA-1 (eBio129c) and PD-L1 (MIH5) were purchased from eBioscience (San Diego, CA). The antibody specific for CCR9 (FAB2160P) was purchased from R&D systems (Minneapolis, MN). FACS analysis and cell sorting were performed using the FACS Canto II (BD Biosciences) and the FACS Aria (BD Biosciences) machines respectively.

2.3. Isolation of LSKs

Bone marrow cells extracted from 6- to 9-week-old C57BL/6 mice were mixed with CD117 MicroBeads (Miltenyi Biotech, Germany), and then $CD117^+$ cells were isolated with the autoMACS Separator (Miltenyi Biotech). The cells were stained with PE-conjugated antibodies specific for the lineage (Gr-1, Mac-1, Ter119, CD3ε, and B220) markers, APC-conjugated c-Kit-, and PE-Cy7-conjugated Sca-1-monoclonal antibodies. After washing, the cells were resuspended in 7-amino-actinomycin (7-AAD) (Calbiochem, San Diego, CA)-containing buffer. The 7-AAD^- $lineage^-$ $Sca\text{-}1^+$ c-Kit^{high} cells were subsequently sorted using the FACS Aria (BD Biosciences). The purity of LSKs was consistently greater than 97%.

2.4. In vitro DC culture

Purified LSKs were cultured in a 48-well flat-bottom culture plate at a density of $4\text{–}10 \times 10^4$ cells/well in IMDM (GIBCO BRL, Grand Island, NY) containing 10% (vol/vol) fetal bovine serum (FBS), penicillin (100 units/ml, Nacalai Tesque, Kyoto, Japan), streptomycin (100 μg/ml, Nacalai Tesque, Kyoto, Japan), murine SCF (100 ng/ml, R&D), and murine TPO (100 ng/ml, R&D) at 37 °C in a humidified air containing 5% CO_2 (pre-culture phase, Fig. 1A). After 48 h, cells were washed, resuspended in IMDM (GIBCO) containing 10% FBS, murine FLT3-ligand (FL) (100 ng/ml, R&D), sodium pyruvate (1 mM, GIBCO), and 2-ME (100 μM, WAKO, Osaka, Japan), seeded in a 96-well round-bottom culture plate at a density of 3×10^3 cells/well, and cultured at 37 °C in a humidified air containing 10% CO_2 for the indicated period (DC-induction phase, Fig. 1A). In an *in vitro* GM-CSF/IL-4-mediated DC (GM/IL-4-DC) culture from LSKs, FL was substituted for GM-CSF (20 ng/ml, R&D) and IL-4 (10 ng/ml, R&D) during the DC-induction phase.

2.5. Plasmid constructs

Using the QuikChange™ Site-Directed Mutagenesis Kit (Stratagene, La Jolla, CA), we constructed a murine FLT3-internal tandem duplication (ITD) that contained a tandem insertion of Arg-Glu-Tyr-Glu-Asp-Lys between amino acids 602/603, similar with the previously reported FLT3-ITD [21]. The primer sequences for FLT3-ITD were as follows: 5′-agg-gaa-tat-gaa-gac-ctt-3′ (forward), 5′-aag-gtc-ttc-ata-ttc-cct-3′ (reverse). Murine FLT3 wild type (FLT3-WT) [22], murine FLT3-ITD, murine $FLT3^{Asp838Val}$ (FLT3-TKD) [22], N-$Ras^{Gly12Asp}$ (CA-N-Ras) [23], murine c-$Kit^{Asp814Val}$ (c-Kit-TKD) [24], FIP1L1/PDGFRα [25], TEL/PDGFRβ [25], AML1/ETO [26], PML/RARα [27], CBFβ/MYH11 [28], AML1dC [29] were each subcloned into a murine stem cell virus-internal ribosome entry site-EGFP (pMie) vector. pMYs-IRES-EGFP, a retrovirus expression vector, was kindly provided by Dr. T. Kitamura (University of Tokyo, Tokyo, Japan). STAT3c [30], 1*6-STAT5A [31], constitutive active form of MEK1 (CA-MEK1) (Invitrogen, Carlsbad, CA, USA), and membrane-targeted p110 [32] were each subcloned into pMYs-IRES-EGFP.

2.6. Preparation of retroviral particles

Conditioned medium containing high titer retroviral particles was prepared as reported previously with some modifications [33]. Briefly, each retroviral vector was cotransfected with vesicular stomatitis virus glycoprotein-, and gag/pol-expression plasmids into 293T cells by Lipofectamine 2000 (Invitrogen). After 48 h, the

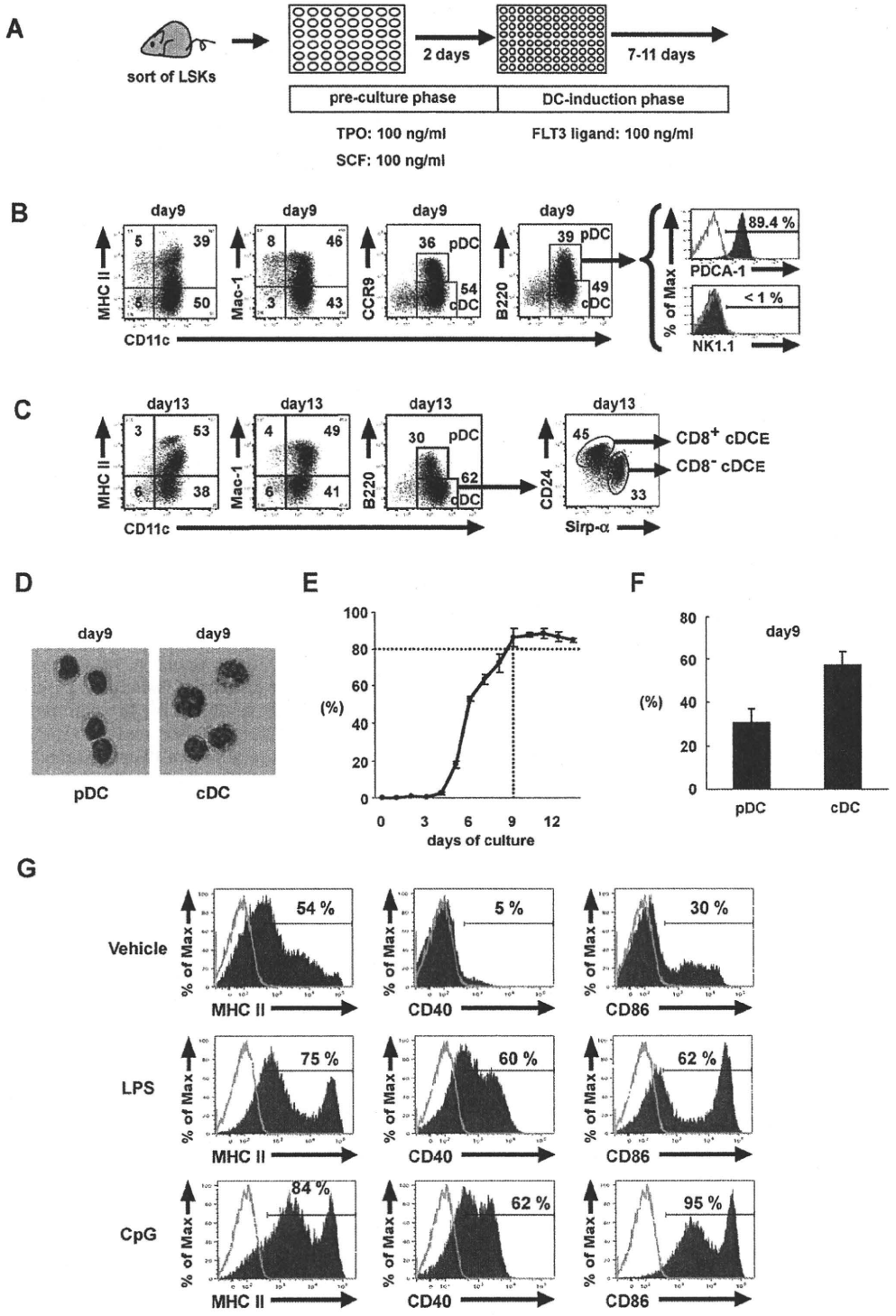

Fig. 1. FL-DCs from LSKs are phenotypically and morphologically similar to FL-DCs from whole bone marrow cells. (A) Schema of an *in vitro* FL-mediated DC differentiation system from LSKs. After 9 (B) or 13 (C) days of culture, cells were collected and the expression of the indicated surface markers was analysed by flow cytometry. (D) After 9 days in culture, FACS-sorted pDCs ($CD11c^+B220^+CCR9^+$) or cDCs ($CD11c^+B220^-CCR9^-$) cells were spun onto slides, and stained with May-Giemsa. Images are shown at ×400 original magnification. (E) Cells were harvested at the indicated day of culture and the surface expression of CD11c was analysed by flow cytometry. (F) After 9 days in culture, cells were collected and the expression of CD11c and B220 was analysed by flow cytometry. The bars show the proportion of pDCs ($CD11c^+B220^+$ cells) and cDCs ($CD11c^+B220^-$ cells) in cultured cells respectively. Numbers in the dot plots represent percentage of cells. (G) After 9 days in culture, cells were stimulated with CpG (1 μM), LPS (1 μg/ml), or left unstimulated. After 24 h, cultured cells were stained with the indicated surface markers and analysed by flow cytometry on the gated $CD11c^+$ cell population. Filled and open histograms show specific staining and back ground staining respectively.

culture supernatant was collected, concentrated 100-fold in volume, filtered (0.45 μm), and aliquoted for storage at −80 C until use.

2.7. Retroviral transduction into murine hematopoietic stem/progenitor cells

Purified LSKs were cultured in IMDM medium (GIBCO) containing 10% FBS, penicillin (100 unit/ml), streptomycin (100 μg/ml), murine SCF (100 ng/ml, R&D), and murine TPO (100 ng/ml, R&D) in a flat-bottom 48-well culture plate at 37 C in a humidified air containing 5% CO_2. After 24 h, cells were seeded into a flat-bottom 48-well culture plate coated with Retronectin (TAKARA BIO, Shiga, Japan) at a density of $1.5–2.0 \times 10^5$ cells/well, and then infected with each retrovirus in the same medium containing protamine sulphate (10 μg/ml, Sigma, St Louis, MO). The cells were cultured at 37 C in a humidified air containing 5% CO_2 for 24 h after which the cells were washed and subjected to the DC-induction phase.

2.8. Allogeneic mixed leukocyte reaction (MLR)

Varying numbers of FACS-sorted, irradiated (30 Gy) *in vitro* FL-mediated $CD11c^+$ or $EGFP^+CD11c^+$ cells were plated in a 96-well round-bottom culture plate with 5×10^4 BALB/c splenic $CD4^+$ T cells that were immunomagnetically selected using the $CD4^+$ T Cell Isolation Kit (Miltenyi Biotec). The purified $CD4^+$ T cells were suspended in a final volume of 150 μl RPMI 1640 (Nacalai Tesque) supplemented with 10% FBS, 2-ME (50 μM), penicillin (100 units/ml, Nacalai Tesque), streptomycin (100 μg/ml, Nacalai Tesque) prior to the mixing reaction. Cells were cultured for 4 days and pulsed with 1 μCi [^{3}H]-thymidine (Amersham Biosciences, Buckinghamshire, UK) per well during the last 16 h of culture. [^{3}H]-thymidine incorporation was measured on a β-plate counter.

2.9. ELISA

To evaluate IFN-α production, more than 97% of purified FL-DCs that were immunomagnetically selected with CD11c microbeads (Miltenyi Biotec), were cultured for 24 h at a density of 5×10^4 cells/200 μl in a 96-well round-bottom culture plate in IMDM medium supplemented with 10% FBS, penicillin (100 units/ml, Nacalai Tesque), streptomycin (100 μg/ml, Nacalai Tesque), 2-ME (50 μM), and sodium pyruvate (1 mM, GIBCO). Cells were stimulated with 1 μM of CpG-A-ODN (5′-ggTGCATCGATGCAgggggG-3′; small letters indicate bases with phosphorothioate-modified backbones), lipopolysaccharide (LPS) (Escherichia coli O55:B5, 1 μg/ml, Sigma, St Louis, MO), or vehicle. Cultured supernatants were assayed using an IFN-α ELISA Kit (R&D systems).

2.10. Cell count

All cultured cells in each well were harvested at 3 or 9 days of culture, and the absolute cell numbers and the proportion of $EGFP^+$ cells were analysed by flow cytometry. Fold increase in $EGFP^+$ cells was obtained by dividing the mean absolute cell numbers of $EGFP^+$ cells in 8 wells at 9 days of culture by the number at 3 days of culture. Data are shown as mean ± standard deviation (SD) from at least three independent assays.

2.11. Statistics

Data are shown as mean ± standard deviation (SD), and the Student *t*-test was used to compare two groups of samples.

3. Results

3.1. Establishment of an in vitro FL-mediated DC differentiation system from LSKs

Our initial aim was to establish a reproducible *in vitro* FL-mediated DC (FL-DC) differentiation system from LSKs for the purpose of assessing the influence of target genes on steady-state DC differentiation. *In vitro* FL-mediated $CD11c^+$ cells from LSKs were subdivided into $CD11c^+B220^+CCR9^+$ cells (pDC phenotype) and $CD11c^+B220^-CCR9^-$ cells (cDC phenotype) (Fig. 1B) [34–37]. $CD11c^+B220^+$ cells also express PDCA-1 but not NK1.1 [38], which is compatible with the pDC phenotype. Consistent with previous studies on FL-DCs from whole bone marrow cells [3,20], FL-DCs from LSKs did not express CD4 or CD8α (data not shown). Additionally $CD11c^+B220^-$ cells could be subdivided into $CD24^{high}CD11b^{low}Sirp\alpha^{low}$ ($CD8^+$ cDC_E) and $CD24^{low}CD11b^{high}Sirp\alpha^{high}$ ($CD8^-$ cDC_E) cells (Fig. 1C), equivalent with $CD8\alpha^+$ and $CD8^-$ cDCs found *in vivo* respectively [20]. FL-DCs from LSKs expressed none or low levels of other lineage markers such as Gr-1, Ter119, CD3ε, CD19, and NK1.1 (data not shown). FL-DCs from LSKs were morphologically compatible with the FL-DCs from whole bone marrow cells (Fig. 1D). After 9 days of culture, greater than 80% of cultured cells were consistently CD11c positive (Fig. 1E). In addition, the proportion of pDCs ($CD11c^+B220^+$ cells) and cDCs ($CD11c^+B220^-$ cells) were reproducibly consistent (pDCs; 30.4 ± 6.4%, cDCs; 57.1 ± 6.4%, pDCs/cDCs ratio; 0.55 ± 0.19) (Fig. 1F). Similar to a previous study using a DC culture from whole bone marrow cells [39], a maximal number of DCs was obtained after 9–10 days of culture (day 9: $7.1 \pm 2.8 \times 10^4$ cells/well), which is similar to the kinetics of FL-induced DC expansion *in vivo* [40]. We next sought to determine the maturation ability of FL-DCs from LSKs. FL-DCs was associated with the upregulation of MHC II and costimulatory molecules upon stimulation with LPS or CpG (Fig. 1G). Similar to *in vitro* DC cultures from whole bone marrow cells, $CD11c^+$ cells included many pre-DCs, defined as $CD11c^+MHC\ II^-$ cells (Fig. 1B and G). Pre-DCs are considered late-stage precursors, and differentiate with a minimal number of divisions into exclusively DC subsets [41,42]. Consistent with this, almost all pre-DCs immediately differentiated into $CD11c^+MHC\ II^+$ cells after 24 h stimulation with CpG or LPS (Fig. 1G). Therefore, we classified all $CD11c^+$ cells, including pre DCs, as FL-DCs. The pDC/cDC ratio did not significantly differ between 9 and 13 days in culture, whereas the proportion of pre-DCs at 13 days of culture was decreased compared to the proportion of pre-DCs at 9 days in culture (Fig. 1B and C). These results were reproducible in at least four independent experiments.

3.2. FL-DCs from LSKs are functional

We next determined whether FL-DCs from LSKs were functional. FL-DCs from LSKs efficiently stimulated allogeneic $CD4^+$ T cells (Fig. 2A). FL-DCs from LSKs yielded a large amount of type I interferon upon CpG-stimulation (Fig. 2B). These results indicated that FL-DCs from LSKs were functionally competent DCs.

3.3. FL-DC differentiation from LSKs is deregulated in a myeloid neoplasm-related gene abnormality-specific manner

Mohty et al. reported the quantitative imbalance of *in vivo* DC subsets in patients with AML and divided the patients into three groups according to the proportion of pDCs and cDCs [13], however, the cause for this heterogeneity was unknown. AMLs have heterogeneous myeloid neoplasm-related gene abnormalities, that are termed class I and class II mutations, which contribute to deregulated signal transduction pathways and myeloid differentiation impairment respectively [43]. On the other hand, DC